

Topological phase transitions in ultra-cold Fermi superfluids: the evolution from BCS to BEC under artificial spin-orbit fields

Kangjun Seo, Li Han and C. A. R. Sá de Melo

School of Physics, Georgia Institute of Technology, Atlanta, Georgia 30332, USA

(Dated: August 25, 2011)

We discuss topological phase transitions in ultra-cold Fermi superfluids induced by interactions and artificial spin orbit fields. We construct the phase diagram for population imbalanced systems at zero and finite temperatures, and analyze spectroscopic and thermodynamic properties to characterize various phase transitions. For balanced systems, the evolution from BCS to BEC superfluids in the presence of spin-orbit effects is only a crossover as the system remains fully gapped, even though a triplet component of the order parameter emerges. However, for imbalanced populations, spin-orbit fields induce a triplet component in the order parameter that produces nodes in the quasiparticle excitation spectrum leading to bulk topological phase transitions of the Lifshitz type. Additionally a fully gapped phase exists, where a crossover from indirect to direct gap occurs, but a topological transition to a gapped phase possessing Majorana fermions edge states does not occur.

PACS numbers: 03.75.Ss, 67.85.Lm, 67.85.-d

Ultra-cold Fermi atoms are one of the most interesting physical systems of the last decade, as they have served as quantum simulators of crossover phenomena and phase transitions encountered in several areas of physics. Due to their tunable interactions, atoms like ^6Li and ^{40}K have been used to study the crossover from BCS to BEC superfluidity, to simulate superfluidity in neutron stars, and to investigate unitary interactions which are of great interest in nuclear physics. Furthermore, the ability to control the internal spin state of the atoms by using radio-frequencies (RF) enabled the studies of quantum and classical phase transitions as a function of interactions and population imbalance. These tools have permitted the study of crossover phenomena and phase transitions, and have validated the symmetry based classification of phase transitions put forth by Landau over the thermodynamic classification proposed earlier by Ehrenfest.

Very recently a new tool for the toolbox was created: artificial spin-orbit coupling has been produced in neutral bosonic systems [1] where the strength of the coupling is controlled optically from weak to strong. The same technique can be applied to ultracold fermions [1] and should allow for the exploration of superfluidity as a function of interactions and fictitious spin-orbit coupling [2]. This possibility created enormous theoretical interest recently [3–9], which was focused on zero temperature (ground state) properties. Considering possible experiments with fermionic atoms such as ^6Li , ^{40}K , we discuss here topological phase transitions at zero and finite temperatures for imbalanced fermions during the evolution from BCS to BEC superfluidity in three dimensions and in the presence of controllable spin-orbit couplings. Even though the symmetry of the order parameter does not change through topological phase transitions, violating Landau's symmetry-based classification, clear signatures emerge in spectroscopic and thermodynamic properties validating Ehrenfest's ideas, which combined with

changes in topological (Hopf) invariants produce a finer classification scheme of phase transitions.

Hamiltonian: We start with the Hamiltonian density

$$\mathcal{H}(\mathbf{r}) = \mathcal{H}_0(\mathbf{r}) + \mathcal{H}_I(\mathbf{r}), \quad (1)$$

where the single-particle term is simply

$$\mathcal{H}_0(\mathbf{r}) = \sum_{\alpha\beta} \psi_{\alpha}^{\dagger}(\mathbf{r}) \left[\hat{K}_{\alpha} \delta_{\alpha\beta} - h_i(\mathbf{r}) \sigma_{i,\alpha\beta} \right] \psi_{\beta}(\mathbf{r}). \quad (2)$$

Here, $\hat{K}_{\alpha} = -\nabla^2/(2m_{\alpha}) - \mu_{\alpha}$ is the kinetic energy in reference to the chemical potential μ_{α} , and $h_i(\mathbf{r})$ is the spin-orbit field along the i -direction ($\alpha = \uparrow, \downarrow$, $i = x, y, z$). The interaction term is $\mathcal{H}_I(\mathbf{r}) = -g\psi_{\uparrow}^{\dagger}(\mathbf{r})\psi_{\downarrow}^{\dagger}(\mathbf{r})\psi_{\downarrow}(\mathbf{r})\psi_{\uparrow}(\mathbf{r})$, where g is a contact interaction, and we set $\hbar = k_B = 1$.

Effective Action: The partition function at temperature T is $Z = \int \mathcal{D}[\psi, \psi^{\dagger}] \exp(-S[\psi, \psi^{\dagger}])$ with action

$$S[\psi, \psi^{\dagger}] = \int d\tau d\mathbf{r} \left[\sum_{\alpha} \psi_{\alpha}^{\dagger}(\mathbf{r}, \tau) \frac{\partial}{\partial \tau} \psi_{\alpha}(\mathbf{r}, \tau) + \mathcal{H}(\mathbf{r}, \tau) \right]. \quad (3)$$

Using the standard Hubbard-Stratanovich transformation that introduces the pairing field $\Delta(\mathbf{r}, \tau) = g\langle\psi_{\downarrow}(\mathbf{r}, \tau)\psi_{\uparrow}(\mathbf{r}, \tau)\rangle$ and integrating over the fermion variables lead to the effective action

$$S_{\text{eff}} = \int d\tau d\mathbf{r} \left[\frac{|\Delta(\mathbf{r}, \tau)|^2}{g} - \frac{T}{2V} \ln \det \frac{\mathbf{M}}{T} + \tilde{K}_{+} \delta(\mathbf{r} - \mathbf{r}') \right],$$

where $\tilde{K}_{+} = (\tilde{K}_{\uparrow} + \tilde{K}_{\downarrow})/2$. The matrix \mathbf{M} is

$$\mathbf{M} = \begin{pmatrix} \partial_{\tau} + \tilde{K}_{\uparrow} & -h_{\perp} & 0 & -\Delta \\ -h_{\perp}^{*} & \partial_{\tau} + \tilde{K}_{\downarrow} & \Delta & 0 \\ 0 & \Delta^{\dagger} & \partial_{\tau} - \tilde{K}_{\uparrow} & h_{\perp}^{*} \\ -\Delta^{\dagger} & 0 & h_{\perp} & \partial_{\tau} - \tilde{K}_{\downarrow} \end{pmatrix}, \quad (4)$$

where $h_{\perp} = h_x - ih_y$ corresponds to the transverse component of the spin-orbit field, h_z to the parallel component with respect to the quantization axis z , $\tilde{K}_{\uparrow} = \hat{K}_{\uparrow} - h_z$, and $\tilde{K}_{\downarrow} = \hat{K}_{\downarrow} + h_z$.

Saddle Point Approximation: To proceed, we use the saddle point approximation $\Delta(\mathbf{r}, \tau) = \Delta_0 + \eta(\mathbf{r}, \tau)$, and write $\mathbf{M} = \mathbf{M}_0 + \mathbf{M}_F$. The matrix \mathbf{M}_0 is obtained via the saddle point $\Delta(\mathbf{r}, \tau) \rightarrow \Delta_0$ which takes $\mathbf{M} \rightarrow \mathbf{M}_0$, and the fluctuation matrix $\mathbf{M}_F = \mathbf{M} - \mathbf{M}_0$ depends only on $\eta(\mathbf{r}, \tau)$ and its Hermitian conjugate. Thus, we write the effective action as $S_{\text{eff}} = S_0 + S_F$. The first term is

$$S_0 = \frac{V}{T} \frac{|\Delta_0|^2}{g} - \frac{1}{2} \sum_{\mathbf{k}, i\omega_n, j} \ln \left[\frac{i\omega_n - E_j(\mathbf{k})}{T} \right] + \sum_{\mathbf{k}} \frac{\tilde{K}_+}{T},$$

in momentum-frequency coordinates $(\mathbf{k}, i\omega_n)$, where $\omega_n = (2n+1)\pi T$. Here, $E_j(\mathbf{k})$ are the eigenvalues of

$$\mathbf{H}_0 = \begin{pmatrix} \tilde{K}_+(\mathbf{k}) & -h_\perp(\mathbf{k}) & 0 & -\Delta_0 \\ -h_\perp^*(\mathbf{k}) & \tilde{K}_-(\mathbf{k}) & \Delta_0 & 0 \\ 0 & \Delta_0^\dagger & -\tilde{K}_+(-\mathbf{k}) & h_\perp^*(-\mathbf{k}) \\ -\Delta_0^\dagger & 0 & h_\perp(-\mathbf{k}) & -\tilde{K}_-(-\mathbf{k}) \end{pmatrix}, \quad (5)$$

which describes the Hamiltonian of elementary excitations in the four-dimensional basis $\Psi^\dagger = \{\psi_\uparrow^\dagger(\mathbf{k}), \psi_\downarrow^\dagger(\mathbf{k}), \psi_\uparrow^\dagger(-\mathbf{k}), \psi_\downarrow^\dagger(-\mathbf{k})\}$. The fluctuation action is

$$S_F = \int d\tau d\mathbf{r} \left[\frac{|\eta(\mathbf{r}, \tau)|^2}{g} - \frac{T}{2V} \ln \det (\mathbf{1} + \mathbf{M}_0^{-1} \mathbf{M}_F) \right].$$

The spin-orbit field is $\mathbf{h}_\perp(\mathbf{k}) = \mathbf{h}_R(\mathbf{k}) + \mathbf{h}_D(\mathbf{k})$, where $\mathbf{h}_R(\mathbf{k}) = v_R(-k_y\hat{\mathbf{x}} + k_x\hat{\mathbf{y}})$ is of Rashba-type [10] and $\mathbf{h}_D(\mathbf{k}) = v_D(k_y\hat{\mathbf{x}} + k_x\hat{\mathbf{y}})$ is of Dresselhaus-type [11], has magnitude $h_\perp(\mathbf{k}) = \sqrt{(v_D - v_R)^2 k_y^2 + (v_D + v_R)^2 k_x^2}$. For Rashba-only (RO) ($v_D = 0$) and for equal Rashba-Dresselhaus (ERD) couplings ($v_R = v_D = v/2$), the transverse fields are $h_\perp(\mathbf{k}) = v_R \sqrt{k_x^2 + k_y^2}$ ($v_R > 0$) and $h_\perp(\mathbf{k}) = v|k_x|$ ($v > 0$), respectively.

Order parameter and number equations: The thermodynamic potential is $\Omega = \Omega_0 + \Omega_F$, where

$$\Omega_0 = V \frac{|\Delta_0|^2}{g} - \frac{T}{2} \sum_{\mathbf{k}, j} \ln \{1 + \exp[-E_j(\mathbf{k})/T]\} + \sum_{\mathbf{k}} \bar{K}_+,$$

with $\bar{K}_+ = [\tilde{K}_+(-\mathbf{k}) + \tilde{K}_-(-\mathbf{k})]/2$ is the saddle point contribution and $\Omega_F = -T \ln Z_F$, with $Z_F = \int \mathcal{D}[\bar{\eta}, \eta] \exp[-S_F(\bar{\eta}, \eta)]$ is the fluctuation contribution. The order parameter is determined via the minimization of Ω_0 with respect to $|\Delta_0|^2$ leading to

$$\frac{V}{g} = -\frac{1}{2} \sum_{\mathbf{k}, j} n_F[E_j(\mathbf{k})] \frac{\partial E_j(\mathbf{k})}{\partial |\Delta_0|^2}, \quad (6)$$

where $n_F[E_j(\mathbf{k})] = 1/(\exp[E_j(\mathbf{k})/T] + 1)$ is the Fermi function for energy $E_j(\mathbf{k})$. We replace the contact interaction g by the scattering length a_s through the relation $1/g = -m_+/(4\pi a_s) + (1/V) \sum_{\mathbf{k}} [1/(2\epsilon_{\mathbf{k},+})]$, where

$m_+ = 2m_\downarrow m_\uparrow/(m_\downarrow + m_\uparrow)$ is twice the reduced mass, $\epsilon_{\mathbf{k},\alpha} = k^2/(2m_\alpha)$ are the kinetic energies, and $\epsilon_{\mathbf{k},+} = [\epsilon_{\mathbf{k},\uparrow} + \epsilon_{\mathbf{k},\downarrow}]/2$. The number of particles for each spin state is $N_\alpha = -\partial\Omega/\partial\mu_\alpha$, which is written as

$$N_\alpha = N_{\alpha,0} + N_{\alpha,F}, \quad (7)$$

where the saddle point contribution is

$$N_{\alpha,0} = -\frac{\partial\Omega_0}{\partial\mu_\alpha} = \frac{1}{2} \sum_{\mathbf{k}} \left[1 - \sum_j n_F[E_j(\mathbf{k})] \frac{\partial E_j(\mathbf{k})}{\partial \mu_\alpha} \right],$$

and the fluctuation contribution is $N_{\alpha,F} = -\partial\Omega_F/\partial\mu_\alpha$.

The self-consistent relations shown in Eqs. (6) and (7) are unphysical for atoms of unequal masses, as it is not possible to have a spin-orbit field that converts atom A into atom B, as this violates barionic number conservation. Therefore, we particularize our discussion to balanced and imbalanced systems of equal masses, where the explicit eigenvalues of the matrix \mathbf{H}_0 are $E_1(\mathbf{k}) = \sqrt{Y_+ + Y_- + 2\sqrt{Y_+ Y_- - |\Delta_0|^2 |h_\perp|^2}}$, which is always positive definite, and $E_2(\mathbf{k}) = \sqrt{Y_+ + Y_- - 2\sqrt{Y_+ Y_- - |\Delta_0|^2 |h_\perp|^2}}$, which can have zeros in momentum space, $E_3(\mathbf{k}) = -E_2(\mathbf{k})$ and $E_4(\mathbf{k}) = -E_1(\mathbf{k})$. Here, $Y_+ = \tilde{K}_+^2(\mathbf{k}) + |\Delta_0|^2 > 0$, $Y_- = \tilde{K}_-^2(\mathbf{k}) + |h_\perp(\mathbf{k})|^2 > 0$, with $\tilde{K}_\pm = (\tilde{K}_\uparrow \pm \tilde{K}_\downarrow)/2$. For equal masses, $K_+ = \epsilon_{\mathbf{k}} - \mu_+$, with $\epsilon_{\mathbf{k}} = k^2/2m$ being the single particle dispersion and $\mu_+ = (\mu_\uparrow + \mu_\downarrow)/2$ being the average chemical potential. Furthermore, $K_- = (\mu_\uparrow - \mu_\downarrow)/2 = \mu_-$ plays the role of a Zeeman field that causes population imbalance $P = N_-/N_+$, where $N_- = N_\uparrow - N_\downarrow$ and $N_+ = N_\uparrow + N_\downarrow$. We define momentum, energy and velocity scales through the total particle density $n_+ = n_\uparrow + n_\downarrow$ or $k_{F+}^3/(3\pi^2) = k_{F\uparrow}^3/(6\pi^2) + k_{F\downarrow}^3/(6\pi^2)$. This choice leads to the Fermi momentum $k_{F+}^3 = (k_{F\uparrow}^3 + k_{F\downarrow}^3)/2$, Fermi energy $\epsilon_{F+} = k_{F+}^2/2m$ and to the Fermi velocity $v_{F+} = k_{F+}/m$.

Phase Diagram: The solutions of Eqs. (6) and (7) subject to thermodynamic stability conditions (positiveness of compressibility matrix $\bar{\kappa}_{\alpha\beta} = (\partial N_\alpha/\partial \mu_\beta)_{T,V}$, isothermal compressibility κ_T and volumetric specific heat C_V) lead to the $T = 0$ phase diagram of population imbalance P versus interaction parameter $1/(k_{F+} a_s)$, which is shown in Fig. 1 for various values of ERD spin-orbit coupling v/v_{F+} . The phase diagram for $v/v_{F+} = 0$ shows a large region where a uniform superfluid US phase is unstable, we call this region NU for possible non-uniform phases including phase separation between superfluid and non-superfluid components or modulated superfluid phases. A general tendency of the phase diagram with increasing spin-orbit coupling v/v_{F+} is the stabilization of superfluid phases and the shrinkage of unstable regions. This stabilization is largely due to the emergence of a triplet component in the order parameter for superfluidity, which circumvents the pair breaking

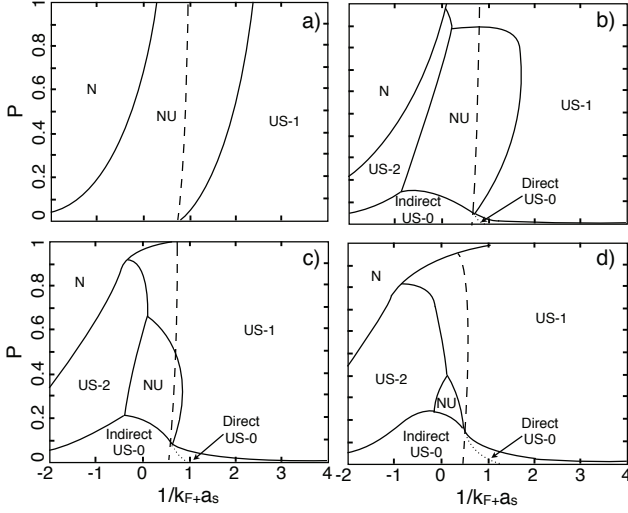


FIG. 1: Phase diagrams of P versus $1/(k_F a_s)$ for ERD spin-orbit couplings: a) $v/v_{F+} = 0$; b) $v/v_{F+} = 0.28$; c) $v/v_{F+} = 0.57$; d) $v/v_{F+} = 0.85$. Solid lines are phase boundaries, the dashed line corresponds to $\mu_+ = 0$, and the dotted line corresponds to a crossover.

abilities of Zeeman fields μ_- . Many multi-critical points and phases exist, including a normal (N) and three uniform superfluid regions: the phase US-0 corresponds to a fully gapped superfluid with no (zero) line of nodes, the phases US-1 and US-2 correspond to gapless superfluids with one-line or two-lines of nodes, respectively. Within the gapped US-0 bulk phase, in our three dimensional system, a topological transition due to emergence of chiral edge states (Majorana fermions) does not occur, instead we have a crossover from indirectly to directly gapped US-0.

Spectroscopic Properties: For the excitation energies $E_1(\mathbf{k})$ and $E_2(\mathbf{k})$, only $E_2(\mathbf{k})$ can have zeros. In the ERD case, where $h_\perp(\mathbf{k}) = v|k_x|$, zeros of $E_2(\mathbf{k})$ can occur for $Y_+ = Y_-$ with $k_x = 0$. This leads to the following cases: (a) two possible lines (rings) of nodes at $(k_y^2 + k_z^2)/(2m) = \mu_+ + \sqrt{\mu_-^2 - |\Delta_0|^2}$ for the outer ring, and $(k_y^2 + k_z^2)/(2m) = \mu_+ - \sqrt{\mu_-^2 - |\Delta_0|^2}$ for the inner ring, when $\mu_-^2 - |\Delta_0|^2 > 0$; (b) doubly-degenerate line of nodes $(k_y^2 + k_z^2)/(2m) = \mu_+$ for $\mu_+ > 0$, doubly-degenerate point nodes for $\mu_+ = 0$, or no-line of nodes for $\mu_+ < 0$, when $\mu_-^2 - |\Delta_0|^2 = 0$; (c) no line of nodes when $\mu_-^2 - |\Delta_0|^2 < 0$. The study of case (a) can be refined into cases (a2), (a1) and (a0). In case (a2), two rings indeed exist provided that $\mu_+ > \sqrt{\mu_-^2 - |\Delta_0|^2}$. However, the inner ring disappears when $\mu_+ = \sqrt{\mu_-^2 - |\Delta_0|^2}$. In case (a1), there is only one ring when $|\mu_+| < \sqrt{\mu_-^2 - |\Delta_0|^2}$. In case (a0), the outer ring disappears at $\mu_+ = -\sqrt{\mu_-^2 - |\Delta_0|^2}$,

and for $\mu_+ < -\sqrt{\mu_-^2 - |\Delta_0|^2}$ no rings exist. Thus, the US-2/US-1 boundary is determined by the condition $\mu_+ = \sqrt{\mu_-^2 - |\Delta_0|^2}$; the US-0/US-2 boundary is determined by the Clogston-like condition $|\mu_-| = |\Delta_0|$ when $\mu_+ > 0$, where the gapped US-0 phase (singlet-rich) disappears leading to the gapless US-2 phase (triplet-rich); and the US-0/US-1 phase boundary is determined by $\mu_+ = -\sqrt{\mu_-^2 - |\Delta_0|^2}$. Furthermore, a crossover line between an indirectly gapped and a directly gapped US-0 phase occurs for $\mu_+ < 0$ and $|\mu_-| = |\Delta_0|$. Lastly, some important multi-critical points arise at the intersections of phase boundaries. First the point $\mu_+ = 0$ and $|\mu_-| = |\Delta_0|$ corresponds to a tri-critical point for phases US-0, US-1, and US-2. Second, the point $|\Delta_0| = 0$ and $\mu_+ = |\mu_-|$ corresponds to a tri-critical point for phases N, US-1 and US-2. Representative excitation spectra are shown in Fig. 2. Near the zeros of $E_2(\mathbf{k})$, quasi-particles have linear dispersion and behave as Dirac fermions. The change in nodal structures is associated with bulk topological transitions of the Lifshitz class as noted for p-wave [12] and d-wave [13] superfluids. The loss of nodal regions correspond to annihilation of Dirac quasi-particles with opposite momenta, which lead to significant changes in spectroscopic properties such as momentum distributions [13] $n_{\mathbf{k},\alpha} = \left[1 - \sum_j n_F[E_j(\mathbf{k})] \partial E_j(\mathbf{k}) / \partial \mu_\alpha\right] / 2$.

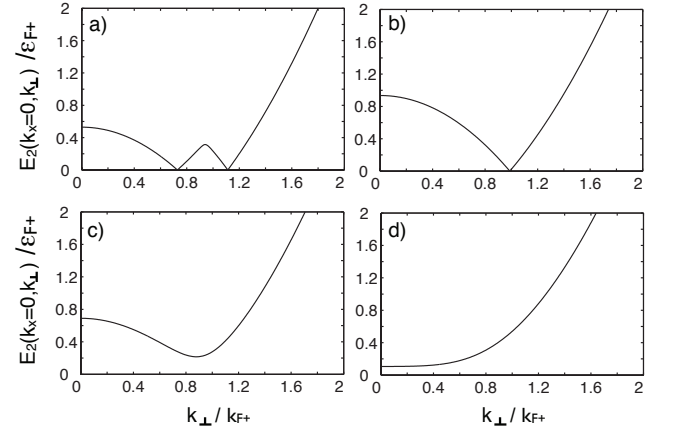


FIG. 2: Excitation energy $E_2(\mathbf{k})/\epsilon_{F+}$ versus k_\perp/k_{F+} , where $k_\perp = \sqrt{k_y^2 + k_z^2}$, for $v/v_{F+} = 0.57$: a) US-2 phase with $P = 0.5$ and $1/(k_F a_s) = -0.92$; b) US-1 phase with $P = 0.5$ and $1/(k_F a_s) = 2.0$; c) US-0 phase (indirect gap) with $P = 0.06$ and $1/(k_F a_s) = -0.5$; and d) US-0 phase (direct gap) with $P = 0.06$ and $1/(k_F a_s) = 0.5$.

Topological Order: The superfluid phases US-0, US-1, US-2 are characterized by different effective actions S_{eff} which depend explicitly on the matrix $\mathbf{M}(i\omega, \mathbf{k}) = [i\omega \mathbf{1} - \mathbf{H}_0(\mathbf{k})]^{-1}$. Setting $i\omega \rightarrow \omega$ and using algebraic topology [14], we construct the topological invariant

$$m = \int_D \frac{dS_\gamma}{24\pi^2} \epsilon^{\mu\nu\lambda\gamma} \text{Tr} [\mathbf{M} \partial_{k_\mu} \mathbf{M}^{-1} \mathbf{M} \partial_{k_\nu} \mathbf{M}^{-1} \mathbf{M} \partial_{k_\lambda} \mathbf{M}^{-1}],$$

which in the gapped US-0 phase is $m = 0$, in the gapless US-1 phase is $m = 1$, and in the gapless US-2 phase is $m = 2$, such that m counts the number of rings in each phase. The integral above has a hyper-surface measure dS_γ and a domain \mathcal{D} that encloses the region of zeros of $\omega = E_j(\mathbf{k}) = 0$. Here $\mu, \nu, \lambda, \gamma$ run from 0 to 3, and k_μ has components $k_0 = \omega$, $k_1 = k_x$, $k_2 = k_y$, and $k_3 = k_z$.

Thermodynamic Properties: To characterize topological phase transitions thermodynamically, we show in Fig. 3 the compressibility matrix $\bar{\kappa}_{\alpha\beta}$ as a function of $1/(k_{F+}a_s)$ for $P = 0.06, 0.14, 0.5, 0.8$ at ERD spin-orbit coupling $v/v_{F+} = 0.57$. Notice that singular behavior occurs at phase boundaries. For instance, in Fig. 3a, $\bar{\kappa}_{\alpha\beta}$ has cusps at the phase boundaries US-2/US-0 and US-0/US-1 and are strictly positive. However, in Fig. 3c, $\bar{\kappa}_{\alpha\beta}$ has discontinuities at the N/US-2 boundary, divergences at the US-2/NU and NU/US-1 boundaries and the diagonal elements $\bar{\kappa}_{\alpha\alpha}$ are negative in the NU region.

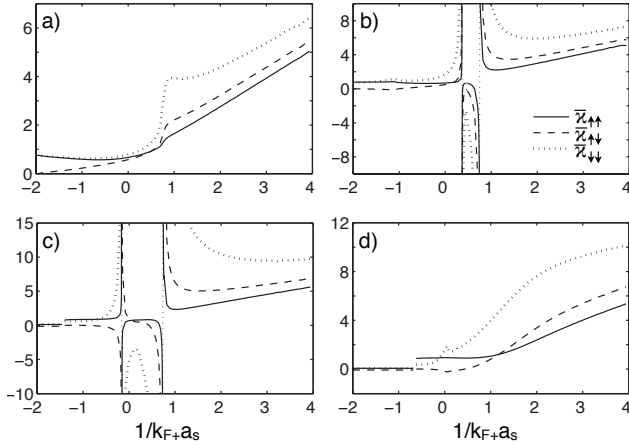


FIG. 3: The $T = 0$ compressibility matrix $\epsilon_{F+}\bar{\kappa}_{\alpha\beta}/N_+$ as a function of $1/(k_{F+}a_s)$ for $v/v_{F+} = 0.57$ at population imbalances a) $P = 0.06$, b) $P = 0.14$, c) $P = 0.50$, d) $P = 0.80$.

Finite Temperatures: As experiments are not performed at $T = 0$, we show in Fig. 4 the P versus T phase diagram at unitarity $1/(k_{F+}a_s) = 0$ for various ERD spin-orbit coupling: a) $v/v_{F+} = 0$; b) $v/v_{F+} = 0.28$; c) $v/v_{F+} = 0.57$; and d) $v/v_{F+} = 0.85$. Phase boundaries are determined by singular behavior of $\bar{\kappa}_{\alpha\beta}$. In Fig. 4, the reduction of the NU region with increasing v/v_{F+} is due to the increasing importance of the triplet component of the order parameter, which stabilizes phases US-1 and US-2 at intermediate and large P .

Conclusions: We have investigated spectroscopic and thermodynamic properties in the BCS-to-BEC evolution at zero and finite temperatures, including spin-orbit effects. We have identified bulk topological phase transitions of the Lifshitz class between gapped and gapless

superfluids and described multi-critical points. In addition, we have found that spin-orbit effects tend to stabi-

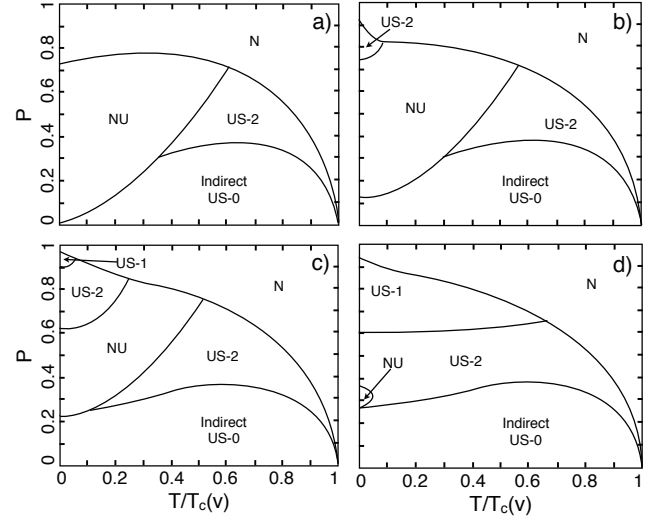


FIG. 4: Phase diagrams of P versus reduced temperature $T/T_c(v)$ at unitarity $1/(k_{F+}a_s) = 0$ for: a) $v/v_{F+} = 0$; b) $v/v_{F+} = 0.28$; c) $v/v_{F+} = 0.57$; d) $v/v_{F+} = 0.85$.

lize uniform superfluid phases against phase separation or non-uniform superfluid phases as population imbalance or interactions are changed, due to the creation of a triplet component in the order parameter that circumvents pair breaking effects due to Zeeman fields.

We thank ARO (W911NF-09-1-0220) for support.

-
- [1] Y. J. Lin, K. Jimenez-Garcia, and I. B. Spielman, *Nature* **471**, 83 (2011).
 - [2] M. Chapman and C. Sá de Melo *Nature* **471**, 41 (2011).
 - [3] J. P. Vyasanakere, Shizhong Zhang, and V. B. Shenoy, arXiv:1104.5633v1 (2011).
 - [4] M. Gong, S. Tewari, C. Zhang, arXiv:1105.1796v1 (2011).
 - [5] Zeng-Qiang Yu, and Hui Zhai, arXiv:1105.2250v1 (2011).
 - [6] H. Hu, L. Jiang, X. Jiu and H. Pu, arXiv:1105.2488v1 (2011).
 - [7] M. Iskin, and A. L. Subasi, arXiv:1106.0473v1 (2011).
 - [8] Li Han, C. A. R. Sá de Melo, arXiv:1106.3613v1 (2011).
 - [9] G. Chen, M. Gong, and C. Zhang, arXiv:1107.2627 (2011).
 - [10] Y. A. Bychkov and E. I. Rashba, *J. Phys. C* **17**, 6029 (1984).
 - [11] G. Dresselhaus, *Phys. Rev.* **100**, 580 (1955).
 - [12] G. E. Volovik, *Exotic Properties of Superfluid ^3He* , World Scientific, Singapore (1992).
 - [13] R. D. Duncan and C. A. R. Sá de Melo, *Phys. Rev. B* **62**, 9675 (2000).
 - [14] M. Nakahara, *Geometry, Topology and Physics*, Adam Hilger, Bristol (1990).